The Plant Journal (2005) **44**, 854–865 doi: 10.1111/j.1365-313X.2005.02581.x

Reviewing models of auxin canalization in the context of leaf vein pattern formation in Arabidopsis

Anne-Gaëlle Rolland-Lagan* **and Przemyslaw Prusinkiewicz**
Department of Computer Science, University of Calgary, 2500 University Drive N.W., Calgary, Alberta, Canada T2N 1N4

Received 17 May 2005; revised 14 August 2005; accepted 8 September 2005.
*For correspondence (fax +1 403 284 4707; e-mail rollanda@cpsc.ucalgary.ca).

Summary

In both plants and animals vein networks play an essential role in transporting nutrients. In plants veins may also provide mechanical support. The mechanism by which vein patterns are formed in a developing leaf remains largely unresolved. According to the canalization hypothesis, a signal inducing vein differentiation is transported in a polar manner and is channeled into narrow strands. Since inhibition of auxin transport affects venation patterns, auxin is likely to be part of the signal involved. However, it is not clear whether the canalization hypothesis, initially formulated over 25 years ago, is compatible with recent experimental data. In this paper we focus on three aspects of this question, and show that: (i) canalization models can account for an acropetal development of the midvein if vein formation is sink-driven; (ii) canalization models are in agreement with venation patterns resulting from inhibited auxin transport and (iii) loops and discontinuous venation patterns can be obtained assuming proper spacing of discrete auxin sources.

Keywords: auxin transport, modeling, canalization, Arabidopsis, pattern formation, leaf venation.

Introduction

Dicotyledonous species exhibit a wide variety of leaf venation patterns (Hickey, 1979). In Arabidopsis the venation forms a complex network composed of veins of different orders. In principle these orders reflect the ontogeny of vein formation: the primary vein (midvein) is formed first followed by the loops of secondary veins (Candela *et al.*, 1999). Finally, higher-order veins differentiate within the loops (Nelson and Dengler, 1997). Nevertheless, there is also evidence that some of the secondary loops visible in adult leaves appear at a later stage and include segments of higher-order veins (Kang and Dengler, 2004).

The mechanism by which veins are formed in a developing leaf is not yet fully understood. Sachs (1969) suggested that formation of veins is induced by auxin as it flows through a tissue. This concept led to the formulation of the canalization hypothesis (Sachs, 1981, 1989): veins are formed in a feedback process, in which differentiation increases the ability of cells to transport the signal that induces this differentiation. Consequently, the signal inducing vein differentiation gets 'canalized' into narrow strands in a process that can be compared with water carving riverbeds in soft terrain (Sachs, 2003). Sachs (1981) suggested that at least part of this signal is auxin. The canalization hypothesis is supported by experiments showing that vein formation depends on auxin and auxin transport (Avsian-Kretchmer *et al.*, 2002; Mattsson *et al.*, 1999; Sieburth, 1999).

The concept of canalization was explored through modeling by Mitchison (Mitchison, 1980, 1981). The models involve a feedback mechanism, in which a parameter of the transport process varies as a function of auxin flux. The strands that drain auxin from the tissue have high flux but low concentration of auxin. Given an initial uniform auxin flow, the development of these strands can be triggered by small random variations in auxin concentration or by localized application of auxin at selected points. Strands of increased auxin flux are assumed to subsequently differentiate into veins. Mitchison further suggested that there is a spatial pattern of localized sources in the leaf, and this pattern is continually changing as the leaf grows (Mitchison, 1980). This assumption made it possible, in particular, to simulate the formation of vein loops. Recent evidence using molecular markers also suggests that auxin sources may be localized (Aloni *et al.*, 2003).

Despite the experimental and theoretical evidence supporting the canalization hypothesis, it still remains unclear whether or not canalization can explain the formation of vein patterns in leaves. Nelson and Dengler (1997) pointed out that the canalization hypothesis could account for open branching patterns but might not be able to account for the network of minor veins. Moreover, at the earliest experimentally revealed stage of vein patterning (the pre-procambial stage, as shown by *Athb8*::GUS expression), midvein formation proceeds acropetally (Scarpella *et al.*, 2004). This acropetal pattern development seems in apparent contradiction with the direction of auxin flow, from the distal part of a leaf towards its base (Dengler, 2001). Doubts were also cast upon the canalization hypothesis by the discovery of mutants with discontinuous venation but relatively normal vein architecture (Berleth, 2000; Deyholos *et al.*, 2000; Koizumi *et al.*, 2000). In particular, Koizumi *et al.* suggested that if the canalization hypothesis were correct any mutation interfering with auxin flow or canal formation should destroy the overall architecture of the vascular pattern. Consequently, they proposed that alternative mechanisms, such as reaction–diffusion (Meinhardt, 1976), should also be investigated.

According to the reaction–diffusion model of vein morphogenesis, a local high concentration of a morphogen (termed the activator) initiates vein differentiation in exposed cells. The differentiated cells remove a substrate substance on which the production of activator depends. As a consequence, differentiation shifts the activator maximum to a neighboring cell, which will differentiate next. Reaction–diffusion is also often considered in a more general (non-vein-specific) sense, as a process in which two or more diffusing substances interact to generate a pattern (e.g. see Koizumi *et al.*, 2000; Nelson and Dengler, 1997). In either the vein-specific or the general case, the limitation of the reaction–diffusion hypothesis is that it assumes diffusive transport of morphogens, whereas auxin transport is known to be polar (Sachs, 1981). In particular, the PIN1 protein, which is a component of the auxin efflux carrier, has a polar location at the plasma membrane (Gälweiler *et al.*, 1998; Steinmann *et al.*, 1999). The altered venation patterns observed in the presence of auxin transport inhibitors or in *pin1* mutants suggest that polar transport is essential for vein pattern formation (Mattsson *et al.*, 1999; Sieburth, 1999). The transport mechanisms involved in vein pattern formation are therefore unlikely to be of a purely diffusive nature, as assumed in reaction–diffusion models.

In this study, we investigate whether or not canalization can account for the features of leaf venation – acropetal midvein formation, loop formation and discontinuous venation observed in mutants – which seem in apparent contradiction with it. We use models of canalization similar to those proposed by Mitchison.

Models

Transport mechanisms

We consider three mechanisms through which a substance *s* can be transported between cells: *s* can move via diffusion, facilitated diffusion or polar transport. Diffusion is a passive transport driven by the concentration gradient, from the cell with a higher concentration of *s* to the cell with a lower concentration. Facilitated diffusion is characterized by the presence of transporters that help carry *s* along the concentration gradient. Polar transport occurs when *s* is carried via transporters in a specific direction, possibly against the concentration gradient.

Canalization equations

In order to model the self-reinforcing process of canalization proposed by Sachs, Mitchison (1980, 1981) considered both facilitated diffusion and polar transport. In either case, he assumed that the transport coefficients (which can be regarded as representing the number of channels or carriers) depend on the flux. An increase in flux would increase the transport coefficient, facilitating further transport.

The original equations for facilitated diffusion (Mitchison, 1980) were, for a flux ϕ of auxin measured from cell *i* to cell *j*:

$$\phi = \tilde{D}(c_i - c_j), \tag{1a}$$

$$\frac{\mathrm{d}\tilde{D}}{\mathrm{d}t} = \alpha\phi^2 + \beta - \gamma\tilde{D}, \tag{1b}$$

where c_i and c_j are the concentrations of auxin in cells *i* and *j*, respectively, and $\tilde{D}$ is a diffusion coefficient. This is similar to the ordinary diffusion equation, except that $\tilde{D}$ is dependent on the flux. $\tilde{D}$ can be interpreted as a measure of the number of channels (or carriers) facilitating transport along the concentration gradient. Parameters α, β and γ are constants: β represents the background production of transporters (channels or carriers) facilitating transport along a concentration gradient, the product $\alpha\phi^2$ is the rate of production of transporters related to the flux, and γ is the rate of decay of transporters. An additional assumption introduced by Mitchison was that values of $\tilde{D}$ higher than a threshold value $\tilde{D}_{\max}$ were clamped to $\tilde{D}_{\max}$.

In the case of polar transport, Mitchison (1980, 1981) proposed several model variants. We used the equations from (Mitchison, 1981) under the assumption that the principal barriers to auxin movement are at the interface between cells (Mitchison, 1980). If the auxin flux is measured in the direction from cell *i* to cell *j*, the equations for polar transport are (the original equations were expressed in terms of parameters ε, *k* and *q*: we rewrite them here in terms

of parameters $\alpha = k\varepsilon$, $\beta = q\varepsilon$ and $\gamma = \varepsilon$, which we find easier to interpret) (Mitchison, 1981):

$$\phi = P_i c_i - P_j c_j, \tag{2a}$$

$$\frac{dP_i}{dt} = \begin{cases} (\alpha\phi^2 + \beta - \gamma P_i) & \text{if } \phi \geq 0 \\ \beta - \gamma P_i & \text{if } \phi < 0, \end{cases} \tag{2b}$$

$$\frac{dP_j}{dt} = \begin{cases} (\alpha\phi^2 + \beta - \gamma P_j) & \text{if } \phi \leq 0 \\ \beta - \gamma P_j & \text{if } \phi > 0, \end{cases} \tag{2c}$$

where P_i and P_j are transport coefficients and α, β and γ are constants. This model can be interpreted in terms of efflux carriers of auxin. Parameter α controls the production of carriers depending on auxin flux, β represents a background production of carriers, and γ represents a decay rate for the efflux carrier. Values of P_i and P_j higher than a threshold value P_{max} are clamped to P_{max}.

The canalization process is thought to be initiated by diffusion (e.g. Koizumi *et al.*, 2005; Mitchison, 1980). In Mitchison's models, passive diffusion is not separated from facilitated diffusion or polar transport. However, if the transport coefficients which vary with the flux are interpreted as a measure of the number of channels or transporters, passive diffusion should be considered a separate parameter. This can be achieved by splitting the transport coefficient $\tilde{D}$ into a background diffusion constant D, and a facilitated diffusion coefficient $\tilde{D}'$. Equations (1) then become:

$$\phi = (D + \tilde{D}')(c_i - c_j), \tag{3a}$$

$$\frac{d\tilde{D}'}{dt} = \alpha\phi^2 + \beta' - \gamma\tilde{D}'. \tag{3b}$$

Similarly, after introducing background diffusion into Equations (2), we obtain:

$$\phi = D(c_i - c_j) + P'_i c_i - P'_j c_j, \tag{4a}$$

$$\frac{dP'_i}{dt} = \begin{cases} (\alpha\phi^2 + \beta' - \gamma P'_i) & \text{if } \phi \geq 0 \\ \beta' - \gamma P'_i & \text{if } \phi < 0, \end{cases} \tag{4b}$$

$$\frac{dP'_j}{dt} = \begin{cases} (\alpha\phi^2 + \beta' - \gamma P'_j) & \text{if } \phi \leq 0 \\ \beta' - \gamma P'_j & \text{if } \phi > 0. \end{cases} \tag{4c}$$

It can be shown that Equations (3) and (4) are equivalent to the original Equations (1) and (2) provided that $\beta - \gamma D = \beta'$ (see Appendix). We observe that, in the presence of passive diffusion, canalization may occur even if the efflux carriers are initially absent ($P_i = P_j = 0$) and there is no background production of these carriers ($\beta' = 0$).

In order to simulate canalization, we used cellular grids as described by Mitchison (1980). Transport of auxin was thus simulated on a two-dimensional rectangular grid of cells of unit area, in which each internal cell (i.e. not lying on the border of the tissue) was assumed to have four neighbors. The concentration c of auxin in each cell varied according to the equation:

$$\frac{dc}{dt} = \sigma + \sum_{k=1}^{n} \phi_k, \tag{5}$$

where σ is the auxin production in the cell (i.e. source activity), n is the number of neighbors and fluxes ϕ_i capture auxin transport between neighboring cells, as described above. At each time step, fluxes between cells were calculated using Equation (1a), (2a), (3a) or (4a), then concentrations were updated using Equation (5), and transport coefficients in all cells were updated using a discretized version of Equations (1b), (2b,c), (3b) or (4b,c). This amounts to solving a system of Equations (1, 5), (2, 5), (3, 5) or (4, 5) using the forward Euler method (Press, 1992). In all cases, the time step was equal to 0.1. All algorithms were written in Matlab (The MathWorks, Inc., Natick, MA, USA).

Parameter values, initial and boundary conditions

Parameter values were chosen so as to match *as closely as possible* the original values proposed by Mitchison (1980). Unless stated otherwise, they were: $\alpha = 5 \times 10^{-5}$, $\beta = 5 \times 10^{-3}$, $\gamma = 5 \times 10^{-2}$ for Equations (1) (Mitchison, 1980), $\alpha = 1 \times 10^{-5}$, $\beta = 5 \times 10^{-3}$, $\gamma = 5 \times 10^{-2}$ for Equation (2), $\alpha = 5 \times 10^{-5}$, $\gamma = 5 \times 10^{-2}$ for Equations (3) $\alpha = 1 \times 10^{-5}$, $\gamma = 5 \times 10^{-2}$ for Equations (4). In Equations (1) and (2), the initial values for transport coefficients $\tilde{D}$, P_i and P_j were 0.325. In Equations (3) and (4), we used $D = 0.325$ for the diffusion constant, the initial values for transport coefficients $\tilde{D}'$, P'_i and P'_j were 0, and the parameter β' was also set to zero (see the Appendix for formulae of equivalence between models). $\tilde{D}_{max}$ (or P_{max}) was set to 4 for all models.

Unless stated otherwise, we used initial and boundary conditions similar to Mitchison (1980). An initial graded distribution of auxin concentrations was set up so that for a cell in row m the initial concentration was equal to $F(m-1)/T_{init}$, where F is a constant ($F = 15$), and T_{init} is the initial value of the transport coefficients ($T = \tilde{D}$, P, $\tilde{D}' + D$, or $P' + D$ for Equations 1, 2, 3 or 4, respectively). Boundary conditions were: a constant influx F of external auxin into the top row of cells, zero auxin concentration in the bottom row (which therefore acts as an auxin sink), and no flux across the left or the right boundary of the tissue.

Equivalence between strands of increased auxin flux and vein differentiation

Simulations describe auxin fluxes, not vein differentiation. At the end of a simulation (equilibrium), strands of increased auxin flux may or may not have reached their maximum canalization capability. The maximum canalization capability is reached when transport coefficients along the strand have reached their maximum value. In our simulations we assumed that strands of increased flux that reached their maximum canalization capability carried enough flux to differentiate into veins. In the case where transport coefficients along the strand did not reach their maximum value, we had to choose a criterion to decide whether the flux would or would not lead to vein differentiation. To do so, we calculated the average influx coming into the cells of the strand, and compared it with the average influx coming into a low flux strand located two cells away (e.g. flux in column 10 of a cell grid would be compared with the flux in column 12 of the grid). A strand of increased flux carrying at least three times more flux than a strand of low flux was considered to lead to vein differentiation.

Results

We reproduced Mitchison's facilitated diffusion model (FD model) and polar transport model (PT model) on rectangular grids of square cells (Figure 1a), using various initial conditions, boundary conditions and different sets of parameter values. In the descriptions, cells are indexed by row number (starting with 1 at the bottom) and by column number (starting with 1 on the left). Auxin fluxes are visualized with arrows, and transport coefficients are visualized using polygons located at the cell walls (Figure 1b–d).

General properties of Mitchison's canalization models

We confirmed Mitchison's result that strands of increased flux emerge as soon as an initially uniform linear gradient of concentrations (Figure 1a) is destabilized (Figure 2a,c). Destabilization was achieved by inducing auxin production ($\sigma > 0$) in one cell for a single time step of the simulation (Figure 2a,c).

We then compared the effect of a transient versus permanent source of auxin on strand formation (Figure 2a–d). If auxin was produced during a single step of simulation, the FD model and the PT model both led to the formation of several strands (Figure 2a,c). In the case where a localized source of auxin was maintained, the FD model led to the formation of several strands (Figure 2b) whereas the PT model generated a single downward strand, attracting a strong flux from the top row of cells (Figure 2d). However,

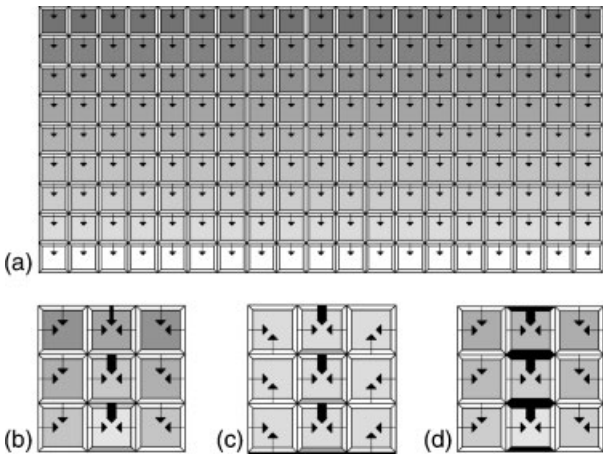

Figure 1. Visualization of auxin flows and concentrations.
Each diagram represents a grid of square cells with their walls. Auxin concentration is color-coded pale to dark gray (blue in Supplementary Material) for low to high concentrations. Arrows represent the direction of auxin flux between cells. Larger fluxes are represented with larger arrows, up to a maximum. Veins are assumed to differentiate in zones of high flux.
(a) Steady state for flux and concentration distribution, in the absence of perturbations.
(b) Iconic representation for the FD model. Diffusion coefficients are color-coded pale to dark gray (red in Supplementary Material) in the walls, and eventually are black when the maximum value is reached.
(c) Iconic representation of the PT model. Similar to (b) except that the efflux coefficients P_i are shown in the four individual walls of each cell. When the transport coefficient has reached its maximum, the wall is shown in black.
(d) Example of a FD model where a strand of high flux has developed and has reached its maximum value (walls are shown in black).

with a much wider grid (33 cells wide), several strands could also develop (not shown). We noted that although the canalization process initially generated lower auxin concentrations (but large fluxes) in the forming strand, later on auxin concentration in the strand could reach higher levels (Figure 2d).

The patterns obtained were sensitive to parameter variations. Increasing the background production of carriers from $\beta = 5 \times 10^{-3}$ (Figure 2a–d) to $\beta = 1.625 \times 10^{-2}$ (Figure 2e–h) delayed or even suppressed strand formation. In particular, in the case of a transient auxin source, the FD model with $\beta = 1.625 \times 10^{-2}$ did not yield stable strands (Figure 2e). Although the PT model with $\beta = 1.625 \times 10^{-2}$ eventually created a strand (Figure 2g), it took much longer to appear than with $\beta = 5 \times 10^{-3}$ (the strand in Figure 2g became visible after 15 000 steps of simulation, whereas in Figure 2c strands became visible shortly before 1600 steps).

These results may be easier to interpret if we reformulate the models to incorporate a background diffusion term (i.e. we use Equations 3 and 4 instead of Equations 1 and 2). For instance, if we set the background production of carriers to zero, models with $\beta = 1.625 \times 10^{-2}$ or $\beta = 5 \times 10^{-3}$ in

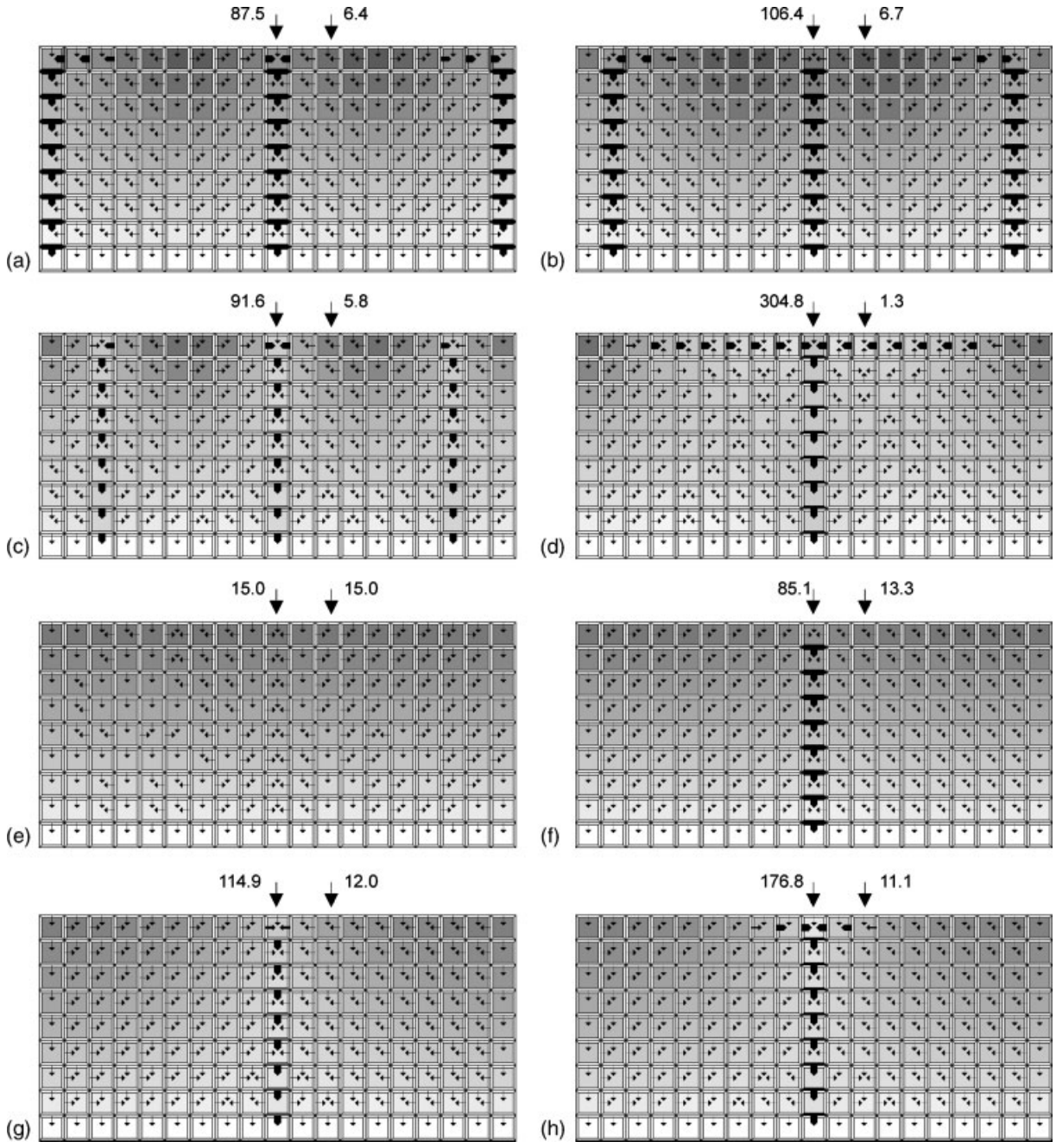

Figure 2. Comparing properties of different canalization models.
Each diagram represents concentrations and fluxes of auxin in a tissue after the system has reached a steady-state (20 000–40 000 steps, depending on the simulation). Arrows above each diagram point to the strands below them. The number near each arrow indicates the average influx in a cell of the strand.
(a,b) Facilitated diffusion using Equations (1) with the default parameter values.
(c,d) Polar transport using Equations (2) with the default parameter values.
(e,f) Facilitated diffusion with $\beta = 1.625 \times 10^{-2}$.
(g,h) Polar transport with $\beta = 1.625 \times 10^{-2}$. In (a), (c), (e) and (g) a transient source of auxin ($\sigma = 50$) was placed in cell (9,10) (top middle cell) for step 1 of the simulation. In (b), (d), (f) and (h) a persistent source of auxin ($\sigma = 50$) was placed in cell (9,10) for the duration of the simulation.

Equations (1) are equivalent to models with $D = 0.1$ and $\tilde{D}_{\text{init}} = 0.225$ or $D = 0.325$ and $\tilde{D}_{\text{init}} = 0$ in Equations (3) (see Models section and formulae for model equivalence in the Appendix). Thus, an increased background diffusion D and a lower initial number of channels delays (and in some cases prevents) strand formation.

Having confirmed the basic properties of Mitchison's canalization models, we applied them to capture specific

features of venation formation in young Arabidopsis leaves. In all cases, we assumed that an increased auxin flux led to vein differentiation (see Models section).

Acropetal formation of the primary vein

Analysis of vein patterning at the pre-procambial stage (Scarpella *et al.*, 2004) suggests that the primary vein is formed acropetally (from leaf base to leaf tip), in spite of auxin being transported basipetally from source to sink. This phenomenon can be reproduced assuming that the formation of the primary vein is sink-driven rather than source-driven. With a single sink cell at the bottom of the tissue and an incoming flux of auxin along the entire top edge of the tissue, a strand of increased flux developed acropetally from the sink towards the top of the tissue (Figure 3a–c and Movie S1 in Supplementary Material). Both FD and PT models produced similar results.

Loop formation

In Arabidopsis, after the primary vein has been formed, secondary veins appear as loops connecting to the primary vein at different points (Figure 4a). This can be modeled using either facilitated diffusion or polar transport, but the models use different sets of assumptions and produce different results.

In the FD model, but not the PT model, loops appeared only if the sink gradually moved away from the initial source to simulate leaf growth, and two new sources were added one after another on both sides of the initial source (Figure 4b and Movie S2 in Supplementary Material). This mode of operation is consistent with the assumption that formation of leaf patterns involves shifting discrete auxin sources (Aloni *et al.*, 2003). The first source of auxin triggers canalization. By the time the second and third sources are added, the cell that contained the first source is already

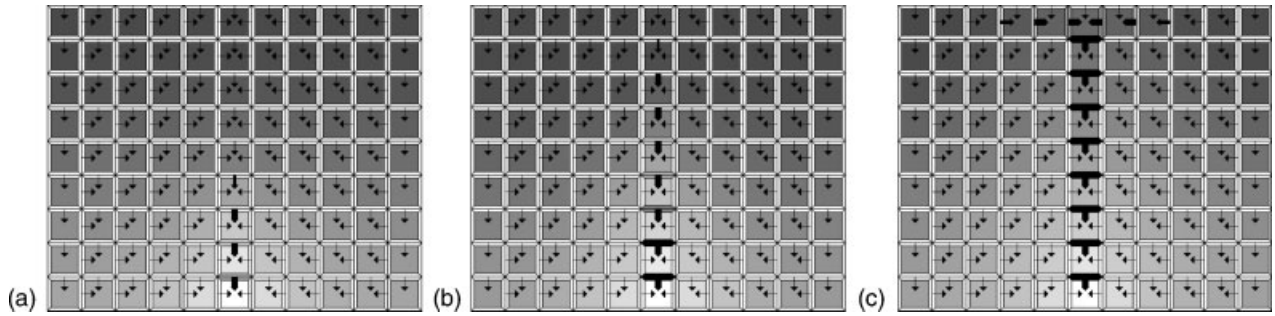

Figure 3. An FD model of acropetal vein formation.
Initial conditions were a linear gradient of concentrations with high concentration at the top and zero concentration at the bottom line of cells. Boundary conditions were a constant flux of auxin coming from the top edge of the tissue, and a sink for auxin ($c = 0$) in cell (1,6).
(a) Simulation is shown at step 500: a strand started forming acropetally.
(b) Step 700 of the simulation: the strand has progressed acropetally.
(c) Step 10 000 of the simulation (steady state has been reached).

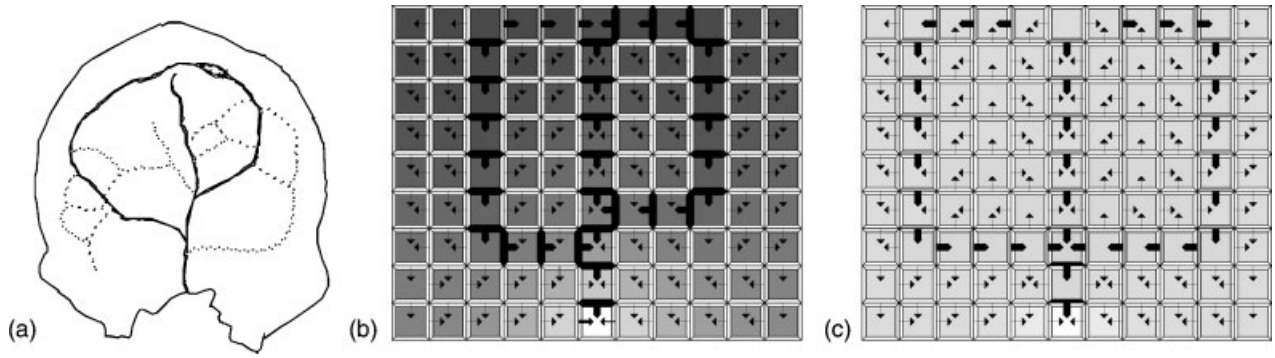

Figure 4. Formation of secondary veins.
(a) Early stage of vein formation in an Arabidopsis leaf, showing the primary vein and the first two loops of secondary veins as full black lines. (Reprinted from Candela, H., Martínez-Laborda, A. and Micol, J.L. (1999) Venation pattern formation in *Arabidopsis thaliana* vegetative leaves. *Dev. Biol.* **205**, 205–216, with permission from Elsevier.)
(b) An FD model of loop formation. Initial concentrations were zero everywhere, and there was no incoming flux of auxin. A first auxin source ($\sigma = 200$) was present in cell (9,6) until step 50, a second auxin source ($\sigma = 200$) was set in cell (9,9) from step 1600 onwards, and a third source ($\sigma = 200$) was set in cell (9,3) from step 2000 onwards. Initially cell (8,6) was a sink, then after every 500 simulation steps the sink was moved down one cell, until the last stage shown at step 4000.
(c) A PT model of loop formation, formulated using Equations (4). Initial concentrations were zero everywhere and there was no incoming flux of auxin. A source ($\sigma = 200$) was set in cells (9,5), (9,6) and (9,7). A sink ($c = 0$) was set in cell (1,6). Simulation is shown at step 10 000 (steady state has been reached).

attracting flux. Auxin from the second and third sources is therefore directed towards both the sink at the base of the leaf and the first source at the top of the leaf. This results in loop formation. The timing of the appearance of each lateral source determines where the corresponding secondary loop will connect to the midvein: a source added later induces a larger loop. We noted that loop formation itself was not very sensitive to the timing and strength of the first source, although varying these parameters affected the timing and direction (basipetal or acropetal) of midvein formation.

In the PT, but not the FD model, loops could be formed without simulating growth, by setting appropriate initial and boundary conditions (Figure 4c). In our experiment, an extended source of auxin (three cell wide) was set at the top of the grid, and all remaining cells initially had no auxin. The model was formulated using Equations (4), using default parameters specified in the Models section, except for $\alpha = 5 \times 10^{-6}$, and $P'_{j,\max} = P'_{i,\max} = 10$. There was no incoming auxin flux on any side of the grid of cells. Unlike the FD model, the PT model did not require several discrete auxin sources. However, we could not find conditions under which the two loops would be asymmetrical: the loops on the left and right side of the midvein always reconnected to the same cell.

Effect of inhibition of auxin transport

Plants treated with an auxin transport inhibitor (1-*N*-naphthylphthalamic acid: NPA) during early leaf development display an altered venation pattern (Mattsson *et al.*, 1999; Sieburth, 1999). In particular, the midvein tends to be wider than normal or to split into several strands, and the veins along the leaf edge are thicker. Severe transport inhibition prevents the midvein from connecting to the base of the leaf (Figure 5a–c). Mattsson *et al.* (1999) interpreted the effects of transport inhibition in terms of auxin canalization, and proposed a diagrammatical representation of auxin fluxes and conductivities under different inhibition conditions. These diagrams were graphical interpretations of the canalization hypothesis, rather than simulation results. We checked the validity of Mattsson *et al.*'s diagrams by incorporating the effect of transport inhibition into Mitchison's models. This was done by reducing the maximum value for transport coefficients, $D_{\max}$ or $P_{\max}$ (depending on the model used). We obtained similar results with the FD and PT models, although in the latter case the maximum value of the transport coefficient, $P_{\max}$, had to be reduced more to see an impact of inhibition of auxin transport on the venation pattern.

Since we only modeled midvein formation, our model of transport inhibition did not account for the higher vein density in this case. Without any inhibition of transport the strand of increased flux representing the prospective midvein (column 6 of the grid in Figure 5d) had an average cell influx of 132.7, as opposed to 9.3 for the cells outside the midvein (grid column 8). Moderate inhibition of transport resulted in a thicker midvein, where the middle strand (column 6, Figure 5e) had an average cell influx of 54.1, compared with 10.8 for the cells in grid column 8. In the case of severe inhibition (Figure 5f), the middle column of cells had an average cell influx of 44.6, compared with 26.4 for the cells in column 8 and 10.2 for the cells of column 10. Flux at the site of the prospective midvein was then considered insufficient (see Models section) to lead to vein formation.

Furthermore, in agreement with diagrams from Mattsson *et al.* (1999), an area of high auxin concentration emerged at the top of the leaf in the case of transport inhibition (Figure 5e,f). This is an area where veins differentiate as a thick band of misshapen tracheary elements (water-conducting cells of the xylem) (Sieburth, 1999).

Vein discontinuities

Mutants have been identified in which vein strands are discontinuous (Carland *et al.*, 1999; Deyholos *et al.*, 2000; Koizumi *et al.*, 2000). For instance, the *van3* mutant (Koizumi *et al.*, 2000, 2005) exhibits a discontinuous vein pattern, although the overall architecture of the venation is preserved (Figure 6a). The discontinuities seem to result from defects in patterning at an early stage, rather than from defects in differentiation (Koizumi *et al.*, 2000, 2005). The existence of such mutants has been seen as an argument against canalization (Koizumi *et al.*, 2000), which was assumed to generate strands in a continuous way. However, under appropriate simulation conditions we observed zones of high flux that extended from both sink and source areas at the same time, with a gap in between (Figure 6b). If the canalization process is stopped before completion of the high-flux strand (e.g. if $\tilde{D}$ is fixed or if differentiation occurs), the strands of high flux will not join and discontinuous veins will be generated (compare Figure 6b and 6c; see also Movie S3 in Supplementary Material). In the presence of several discrete auxin sources in the leaf blade, canalization could therefore lead to the formation of discontinuous strands.

Discussion

The role of background diffusion

In the original canalization models (Mitchison, 1980, 1981), one transport coefficient, which varies with the flux, represents both the background diffusion and the facilitated diffusion or polar transport between cells. We proposed a modified expression of the canalization equations, in which background diffusion is introduced explicitly into the models. Mathematically, the original and modified equations are equivalent, provided that the parameters are adjusted accordingly. Nevertheless, some results are easier to state or

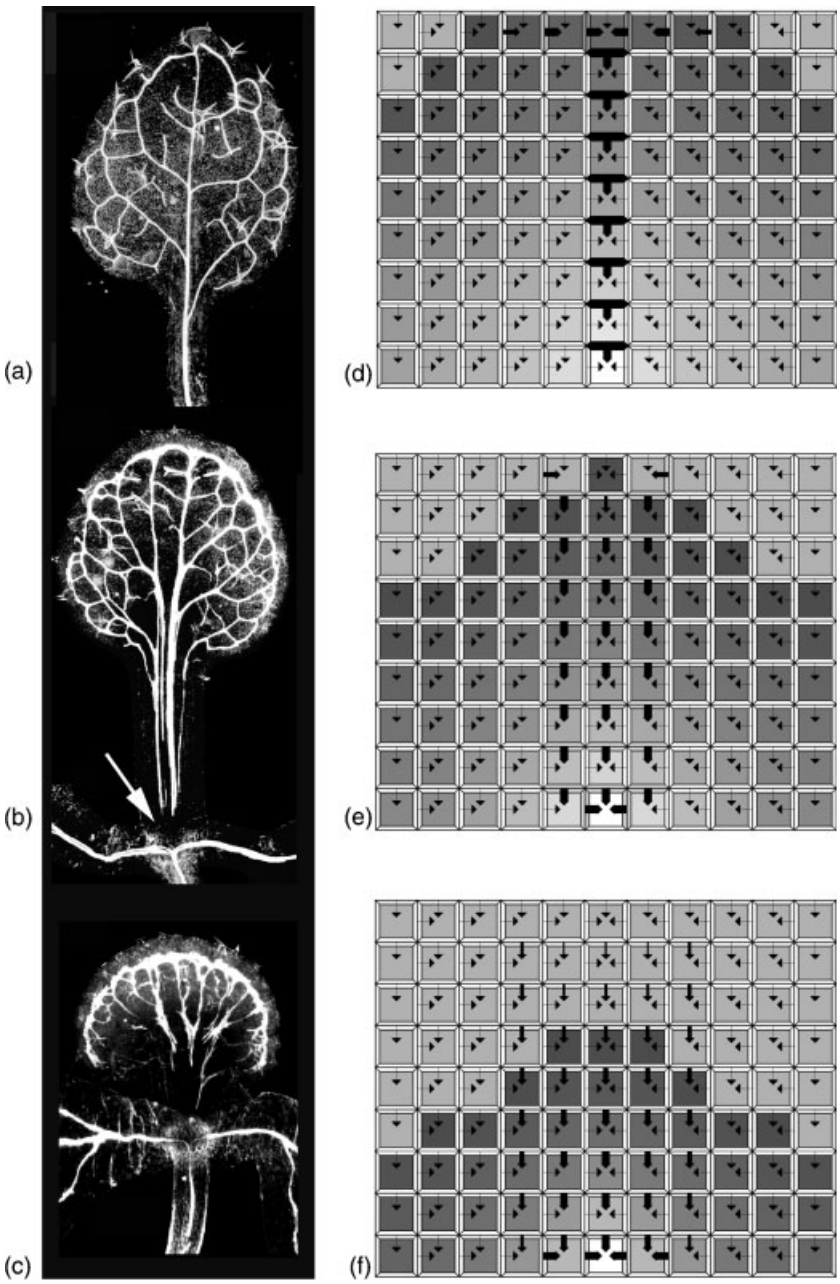

Figure 5. Modeling the effects of auxin transport inhibition.
(a–c) Arabidopsis leaf venation patterns resulting from a treatment with transport inhibitor (NPA): (a) control, (b) mild inhibition, (c) severe inhibition. (Reproduced from Mattsson *et al.* (1999) with permission from The Company of Biologists Ltd.)
(d–f) Modeling the effects of reduced transport. Initial conditions were a linear gradient of concentrations, with high concentrations at the top and zero concentrations at the bottom line of cells. Boundary conditions were a constant flux of auxin coming from the top edge of the tissue, and a sink for auxin ($c = 0$) in cell (1,6). The highest concentrations of auxin at the top of the grid are shown in lighter gray. Simulations are shown at step 10 000 of the simulation (steady state has been reached): (d) same as Figure 3(c) (normal transport: $D_{max} = 4$), (e) same as (d) with $D_{max} = 1$, (f) same as (d) with $D_{max} = 0.5$. For comparison purposes, the color code for transporters was set from pale to dark gray for values ranging from 0 to 4 (black walls for $\tilde{D} = 4$), instead of 0 to D_{max}.

interpret by referring to the background diffusion. Specifically, with a lower background diffusion and higher initial number of channels/carriers, the tissue is more sensitive to small perturbations (e.g. a highly transient source of auxin). Without background diffusion, the presence of a single auxin source can lead to the formation of a pattern of approximately evenly spaced strands of high flux. On the other hand, with increased background diffusion, strand formation can be limited to a connection between source and sink: we did not observe the formation of multiple strands in that case even for wide grids (e.g. 49 cells wide, results not shown). The above results indicate that background diffusion may play an important role in controlling the formation of veins that connect sources to sinks.

Acropetal vein formation

According to the simulations, a uniform incoming auxin flux along the top edge of the forming leaf and a localized sink at the base cause the primary vein to form acropetally. The model thus shows that there is no necessary contradiction between an acropetal development of the midvein and the basipetal direction of auxin flow. Furthermore, the model suggests that in the early stages of primordium formation,

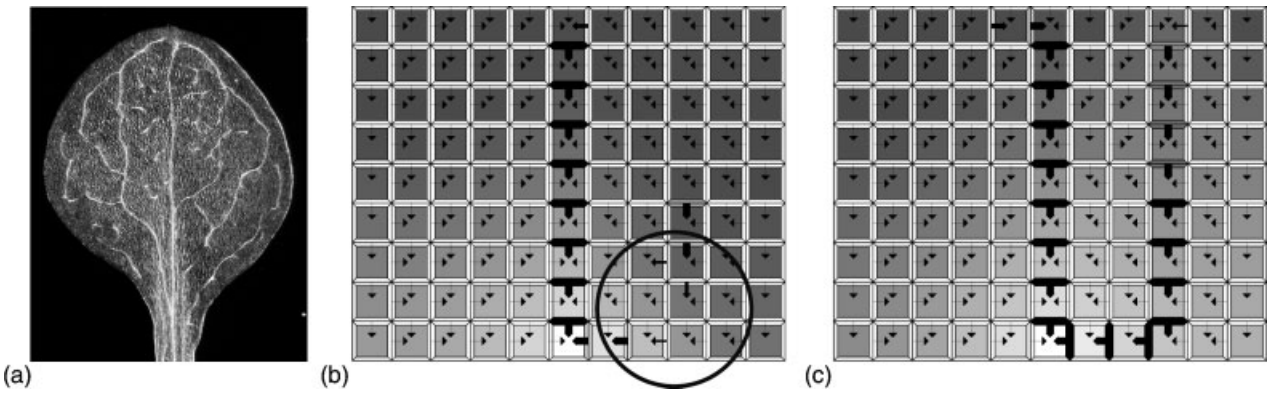

Figure 6. Canalization and discontinuous venation.
(a) Discontinuous vasculature in a first rosette leaf of a *van3* Arabidopsis mutant. (Reproduced from Koizumi *et al.* (2000) with permission from The Company of Biologists Ltd.)
(b) Illustration of discontinuities during strand formation. Initial concentrations were zero and there was an influx of auxin from the top of the grid. Two sources were set at step 1 and maintained throughout the simulation. The first source ($\sigma = 100$) was set in cell (9,6), and the second source ($\sigma = 50$) was set in cell (5,9). Simulation is shown at step 1600: the strand between the second source and the sink has started to form both from the sink and from the source. This strand is discontinuous (see area inside the black circle). If canalization is interrupted at that stage by fixing $\bar{D}$, the two strands of high flux will not join, leading to discontinuous veins when differentiation occurs.
(c) Same as (b) after 10 000 steps: if the canalization is not interrupted, the discontinuous strands eventually connect to form continuous veins.

there are no localized auxin sources and that it is the presence of the sink that drives strand formation. This is consistent with experimental data suggesting that, during early leaf formation, auxin is not produced in the primordium (Avsian-Kretchmer *et al.*, 2002), but flows towards it via the epidermal layer (L1) (Reinhardt *et al.*, 2003). In our model, this would correspond to the auxin flow from L1 to the top row of cells in the grid.

Effects of transport inhibition

Our models of transport inhibition during midvein formation gave similar results to the diagrammatical interpretation proposed by Mattsson *et al.* (1999). However, neither the model nor the diagrams capture the loss of connection between the midvein and the base of the leaf observed experimentally (Mattsson *et al.*, 1999, see Figure 5b,c). This absence of connection between midvein and leaf base will need to be investigated further, both by experimental and model studies.

Localization of auxin sources and the role of growth

We showed that localized auxin sources are compatible with the existence of mutants with discontinuous veins. We also showed that localized auxin sources can induce realistic loop patterns in a growing leaf. This suggests that localized auxin sources acting in a growing leaf may play an important role in the formation of vein patterns.

It is still unclear where in the leaf auxin is produced. Expression of the auxin-responsive reporter gene *DR5*::GUS (Ulmasov *et al.*, 1997) is often used to visualize sites of high auxin concentration, and seems to match results from auxin immunolocalization (Benková *et al.*, 2003). However, the activation of *DR5* in the presence of auxin does not provide a proof that the sites of high *DR5*::GUS expression coincide with the sites of auxin production. That being said, *DR5*::GUS is expressed in a dotted pattern in the areas where veins are about to form (Koizumi *et al.*, 2005). This is consistent with the model assumption that auxin sources are localized. In the *van3* mutant, the density of the dots is reduced compared with the wild type (Koizumi *et al.*, 2005). The lower density of sources in the *van3* mutant may imply that differentiation occurs before canalization is complete, resulting in discontinuous vein patterns.

The hypothesis of highly localized auxin sources, or localized areas of high auxin production amongst other auxin-producing cells, leads to the questions of what mechanisms might be responsible for the spatial and temporal pattern of auxin source distribution and production. While morphogenetic mechanisms such as reaction–diffusion can be contemplated, at present the answer to these questions is not known. In a recently proposed model (Runions *et al.*, 2005), the formation of new auxin sources is inhibited by the proximity of existing auxin sources and veins. As the leaf grows, new auxin sources thus appear at locations sufficiently distant from both the existing sources and veins. This model reproduced a range of venation patterns in a visually realistic manner.

Flux versus concentration

Although it has been shown that veins can differentiate in tissues exposed to auxin (Sachs, 1981), it remains unclear whether vein formation responds to high auxin concentrations or high auxin fluxes. While the *DR5*::GUS expression

pattern suggests the former interpretation, this is not a definitive conclusion, since the *DR5* reporter may be inadequate to distinguish between high auxin concentrations and high fluxes.

Mathematical models of canalization proposed by Mitchison (1980, 1981) simulate vein formation as a result of high fluxes. However, in the case of inhibition of auxin transport, thick veins form at the leaf margin, where auxin seems to accumulate instead of being efficiently channeled away (Mattsson *et al.*, 1999). This is confirmed by our simulations, which showed that when transport is impaired, the margin of the leaf is an area of low fluxes and high auxin concentrations. This suggests that vein differentiation at the margins can be caused by high auxin concentrations in spite of low fluxes. This apparent inconsistency might be solved by assuming that vein differentiation results from being exposed to a sufficient number of auxin molecules. This can be achieved by a long exposure to a large number of molecules (high concentration, low flux), or a rapid turnover of exposure to a smaller number of molecules (high flux, low concentration). Veins could then form both due to prolonged high auxin concentrations or high auxin fluxes. Specifically, in Figure 5(e,f), zones of increased concentrations (lighter gray at the top of the grid) would form thick veins at the margin, whereas zones of high flux would form veins extending towards the base of the leaf. Note that low fluxes give weaker directional information, which could be the reason why some tracheary elements at the leaf margin are misshapen and rounded instead of being normally elongated (Sieburth, 1999).

Molecular mechanisms underlying canalization

Canalization of auxin can be modeled using facilitated diffusion or polar transport. Both classes of model are capable of generating a large variety of patterns. In both types of model robust patterns seem to emerge more easily if background diffusion is also present. This suggests that background diffusion may be responsible for the onset of facilitated diffusion or polar transport.

It is still unclear how the canalization equations of the facilitated diffusion and polar transport models relate to the molecular mechanisms of auxin transport. In both types of models transport increases as a function of the net flux squared (the relation between transport coefficients and flux needs to be non-linear for canalization to proceed). In facilitated diffusion models, the increase in transport coefficients depends on flux direction, but is independent of flux orientation. It is therefore possible that polarity only plays an indirect role in canalization. Nevertheless, molecular data currently seem to give more support to the polar models.

Canalization models imply a feedback between auxin transport and the localization of transporters at the cell membrane. This is consistent with the idea that auxin flux can both polarize the cells and maintain their polarity (Sachs, 1981). In the polar transport models presented here, the localization of carriers at one end of the cell mimics the polar localization of the PIN1 protein. PIN1 is a component of the auxin efflux carrier and has a polar location at the plasma membrane of vascular cells (Gälweiler *et al.*, 1998; Steinmann *et al.*, 1999). Furthermore, it has been shown that PIN1 relocalizes upon application of auxin (Benková *et al.*, 2003; Peer *et al.*, 2004), and it was recently shown that auxin regulates the abundance of PIN at the cell membrane (Paciorek *et al.*, 2005). These observations raise the possibility that the presence and localization of PIN1 might be regulated by auxin flux in the same way as the carriers of the canalization models presented here. Factors other than PIN1 may be involved in the canalization process during leaf morphogenesis, including other PIN proteins (e.g. several PIN proteins are involved in auxin transport in the root (Blilou *et al.*, 2005)), influx carriers (Kramer, 2005; Swarup *et al.*, 2000), AtMDR/PGP proteins (Noh *et al.*, 2003) and the protein serine–threonine kinase PINOID (PID) (Friml *et al.*, 2004). In order to relate current models to molecular mechanisms, experimental data are needed to assess patterns of expression of efflux carriers, influx carriers and PINOID in a variety of experimental scenarios (wild type, mutants, conditions of inhibited transport).

The general properties of the auxin canalization models proposed by Mitchison 25 years ago remain relevant to the current studies of formation of vein patterns. Examined separately, variants of Mitchison's models are consistent with several features of Arabidopsis venation. The proposed FD model of loop formation comes the closest to integrating all elements: the midvein forms acropetally and strands of increased flux are initially discontinuous, before joining up. However, a limitation of this particular model is that growth is only simulated by moving the auxin sink, rather than by modeling growth itself. Moreover, the different models presented here used different initial and boundary conditions (see figure legends for the initial and boundary conditions of each model), and available experimental data are at present insufficient to decide which conditions would be the most realistic ones. Lastly, it remains unclear whether a polar (PT) or axial (FD) model would be best suited to account for canalization in leaves. Recent modeling studies have also shown that canalization can be modeled in different ways, so that veins may form in areas of high fluxes but either high or low concentrations (Feugier *et al.*, 2005). Incorporating a more accurate simulation of leaf growth and taking into account new molecular data may make it possible to improve the presented models, and consequently lead to a better understanding of auxin distribution/transport and vein pattern formation.

In reaction–diffusion, morphogens act by controlling their rates of production, or those of other morphogens, through feedback mechanisms. By contrast, in the models presented

here, morphogens act by modifying the parameters of the transport process. Such models can be viewed as a class of pattern formation mechanisms on their own, perhaps complementary to reaction–diffusion.

Acknowledgements

We thank Pavol Federl for participating in early stages of this work, and Thomas Berleth for helpful comments. We further thank Jose Luis Micol for Figure 4(a), Jim Mattsson and Thomas Berleth for Figure 5(a–c), and Hiroo Fukuda and Koji Koizumi for Figure 6(a). We gratefully acknowledge the support from Alberta Ingenuity and the Pacific Institute for the Mathematical Sciences to A.-G.R.-L.; and support from the Natural Sciences and Engineering Research Council of Canada, and the Human Frontier Science Program to P.P.

Supplementary Material

The following supplementary material is available for this article online:

Movie S1. Acropetal development of a strand of high flux using the FD model, corresponding to Figure 3. The simulation was carried out for 3000 steps, and the movie records every 100th step.

Movie S2. Loop formation using the FD model, corresponding to Figure 4b. The simulation was carried out for 8000 steps, when the equilibrium was reached. (Note Figure 4b shows an earlier stage of loop formation, corresponding to step 4000, when leaf growth has stopped.) The simulation shows that, at the equilibrium, carriers along the strands operate at their maximum carrying capacity, and the additional auxin flux from the loops causes an increase in the midvein width from the points where the loops join the midvein toward the base. The movie shows every 100th simulation step.

Movie S3. Formation of discontinuous strands using the FD model, corresponding to Figure 6(b,c). The strand linking the source on the left to the sink develops both from source to sink and from sink to source, therefore the strand is initially discontinuous. The simulation was carried out for 4000 steps, and the movie records every 100th step.

This material is available as part of the online article from http://www.blackwell-synergy.com

References

Aloni, R., Schwalm, K., Langhans, M. and Ullrich, C.I. (2003) Gradual shifts in sites of free-auxin production during leaf-primordium development and their role in vascular differentiation and leaf morphogenesis in Arabidopsis. *Planta*, **216**, 841–853.

Avsian-Kretchmer, O., Cheng, J.-C., Chen, L., Moctezuma, E. and Sung, Z.R. (2002) Indole acetic acid distribution coincides with vascular differentiation pattern during Arabidopsis leaf ontogeny. *Plant Physiol.* **130**, 199–209.

Benková, E., Michniewicz, M., Sauer, M., Teichmann, T., Seifertová, D., Jürgens, G. and Friml, J. (2003) Local, efflux-dependent auxin gradients as a common module for plant organ formation. *Cell*, **115**, 591–602.

Berleth, T. (2000) Plant development: Hidden networks. *Curr. Biol.* **10**, R658–R661.

Blilou, I., Xu, J., Wildwater, M., Willemsen, V., Paponov, I., Friml, J., Heidstra, R., Aida, M., Palme, K. and Scheres, B. (2005) The PIN auxin efflux facilitator network controls growth and patterning in Arabidopsis roots. *Nature*, **433**, 39–44.

Candela, H., Martínez-Laborda, A. and Micol, J.L. (1999) Venation pattern formation in Arabidopsis thaliana vegetative leaves. *Dev. Biol.* **205**, 205–216.

Carland, F.M., Berg, B.L., FitzGerald, J.N., Jinamornphongs, S., Nelson, T. and Keith, B. (1999) Genetic regulation of vascular tissue patterning. *Plant Cell*, **11**, 2123–2137.

Dengler, N. (2001) Regulation of vascular development. *J. Plant Growth Regul.* **20**, 1–13.

Deyholos, M.K., Cordner, G., Beede, D. and Sieburth, L.E. (2000) The SCARFACE gene is required for cotyledon and leaf vein patterning. *Development*, **127**, 3205–3213.

Feugier, F.G., Mochizuki, A. and Iwasa, Y. (2005) Self-organization of the vascular system in plant leaves: inter-dependent dynamics of auxin flux and carrier proteins. *J. Theor. Biol.* **236**, 366–375.

Friml, J., Yang, X., Michniewicz, M. *et al.* (2004) A PINOID-dependant binary switch in apical-basal PIN polar targeting directs auxin efflux. *Science*, **306**, 862–865.

Gälweiler, L., Guan, C., Müller, A., Wisman, E., Mendgen, K., Yephremov, A. and Palme, K. (1998) Regulation of polar auxin transport by AtPIN1 in Arabidopsis vascular tissue. *Science*, **282**, 2226–2230.

Hickey, L.J. (1979) A revised classification of the architecture of dicotyledonous leaves. In *Anatomy of Dicotyledons* (Metcalfe, C.R. and Chalke, L., eds), Vol. 1. New York: Oxford University Press, pp. 25–39.

Kang, J. and Dengler, N. (2004) Vein pattern development in adult leaves of Arabidopsis thaliana. *Int. J. Plant Sci.* **165**(2), 231–242.

Koizumi, K., Sugiyama, M. and Fukuda, H. (2000) A series of novel mutants of Arabidopsis thaliana that are defective in the formation of continuous vascular network: calling the auxin signal flow canalization hypothesis into question. *Development*, **127**, 3197–3204.

Koizumi, K., Naramoto, S., Sawa, S., Yahara, N., Ueda, T., Nakano, A., Sugiyama, M. and Fukuda, H. (2005) VAN3 ARF-GAP-mediated vesicle transport is involved in leaf vascular network formation. *Development*, **132**, 1699–1711.

Kramer, E.M. (2005) PIN and AUX/LAX proteins: their role in auxin accumulation. *Trends Plant Sci.* **9**, 578–582.

Mattsson, J., Sung, Z.R. and Berleth, T. (1999) Responses of plant vascular systems to auxin transport inhibition. *Development*, **126**, 2979–2991.

Meinhardt, H. (1976) Morphogenesis of lines and nets. *Differentiation*, **6**, 117–123.

Mitchison, G.J. (1980) A model for vein formation in higher plants. *Proc. R. Soc. Lond. B*, **207**, 79–109.

Mitchison, G.J. (1981) The polar transport of auxin and vein patterns in plants. *Philos. Trans. R. Soc. Lond. B*, **295**, 461–471.

Nelson, T. and Dengler, N. (1997) Leaf vascular pattern formation. *Plant Cell*, **9**, 1121–1135.

Noh, B., Bandyopadhyay, A., Peer, W.A., Spalding, A.P. and Murphy, A.S. (2003) Enhanced gravi- and phototropism in plant mdr mutants mislocalizing the auxin efflux protein PIN1. *Nature*, **423**, 999–1002.

Paciorek, T., Zažímalová, E., Ruthardt, N. *et al.* (2005) Auxin inhibits endocytosis and promotes its own efflux from cells. *Nature*, **435**, 1251–1256.

Peer, W.A., Bandyopadhyay, A., Blakeslee, J.J., Makam, S.N., Chen, R.J., Masson, P.H. and Murphy, A.S. (2004) Variation in expression and protein localization of the PIN family of auxin efflux facilitator proteins in flavonoid mutants with altered auxin transport in Arabidopsis thaliana. *Plant Cell*, **16**, 1898–1911.

Press, W.H. (1992) *Numerical Recipes in C: the Art of Scientific Computing*. Cambridge: Cambridge University Press, 994 pp.

Reinhardt, D., Pesce, E.R., Stieger, P., Mandel, T., Baltensperger, K., Bennett, M., Traas, J., Friml, J. and Kuhlemeier, C. (2003) Regulation of phyllotaxis by polar auxin transport. *Nature*, **426**, 255–260.

Runions, A., Fuhrer, M., Lane, B., Federl, P., Rolland-Lagan, A.-G. and Prusinkiewicz, P. (2005) Modeling and visualization of leaf venation patterns. *ACM Trans. Graphics*, **24**(3), 702–711.

Sachs, T. (1969) Polarity and the induction of organized vascular tissues. *Ann. Bot.* **33**, 263–275.

Sachs, T. (1981) The control of the patterned differentiation of vascular tissues. *Adv. Bot. Res.* **9**, 151–162.

Sachs, T. (1989) The development of vascular networks during leaf development. *Curr. Top. Plant. Biochem. Physiol.* **8**, 168–183.

Sachs, T. (2003) Collective specification of cellular development. *BioEssays*, **25**, 897–903.

Scarpella, E., Francis, P. and Berleth, T. (2004) Stage-specific markers define early steps of procambium development in Arabidopsis leaves and correlate termination of vein formation with mesophyll differentiation. *Development*, **131**, 3445–3455.

Sieburth, L.E. (1999) Auxin is required for leaf vein pattern in Arabidopsis. *Plant Physiol.* **121**, 1179–1190.

Steinmann, T., Geldner, N., Grebe, M., Mangold, S., Jackdon, C.L., Paris, S., Gälweiler, L., Palme, K. and Jürgens, G. (1999) Coordinated polar localization of auxin efflux carrier PIN1 by GNOM ARF GEF. *Science*, **286**, 316–318.

Swarup, R., Marchant, A. and Bennett, M.J. (2000) Auxin transport: providing a sense of direction during plant development. *Biochem. Soc. Trans.* **28**, 481–485.

Ulmasov, T., Murfett, J., Hagen, G. and Guilfoyle, T.J. (1997) Aux/IAA proteins repress expression of reporter genes containing natural and highly active synthetic auxin response elements. *Plant Cell*, **9**, 1963–1971.

Appendix: Equivalence between diffusive and non-diffusive models

We can show that Equations (3) are equivalent to Equations (1) in the original model. To do so, we substitute $D + \tilde{D}'$ for $\tilde{D}$ in Equations (1), which then become:

$$\phi = (D + \tilde{D}')(c_i - c_j),$$

$$\frac{\mathrm{d}\tilde{D}}{\mathrm{d}t} = \frac{\mathrm{d}D}{\mathrm{d}t} + \frac{\mathrm{d}\tilde{D}'}{\mathrm{d}t} = \frac{\mathrm{d}\tilde{D}'}{\mathrm{d}t} = \alpha\phi^2 + \beta - \gamma D - \gamma\tilde{D}'.$$

We now see that Equations (1) are equivalent to Equations (3), provided that $\beta - \gamma D = \beta'$. Furthermore, the initial conditions and threshold values must be adjusted according to the equation $D + \tilde{D}' = \tilde{D}$, yielding:

$$\tilde{D}'_{\text{init}} = \tilde{D}_{\text{init}} - D,$$

$$\tilde{D}'_{\max} = \tilde{D}_{\max} - D.$$

This provides an easy way to translate one model into another. For instance, the FD model can be reformulated as a model with background diffusion, by choosing β' or D such that :

$$D = \frac{\beta - \beta'}{\gamma}; \quad \tilde{D}'_{\text{init}} = \tilde{D}_{\text{init}} - D; \quad \tilde{D}'_{\max} = \tilde{D}_{\max} - D;$$

where $\tilde{D}'_{\text{init}}$ and $\tilde{D}_{\text{init}}$ are values for $\tilde{D}'$ and $\tilde{D}$ at the start of the simulation.

In an analogous way, we can show that Equations (4) are equivalent to Equations (2) in the original model. To do so, we substitute $D + P'_i$ for P_i and $D + P'_j$ for P_j in Equations (2), which then become:

$$\phi = (D + P'_i)c_i - (D + P'_j)c_j,$$

$$\frac{\mathrm{d}P_i}{\mathrm{d}t} = \frac{\mathrm{d}D}{\mathrm{d}t} + \frac{\mathrm{d}P'_i}{\mathrm{d}t} = \frac{\mathrm{d}P'_i}{\mathrm{d}t} = \begin{cases} (\alpha\phi^2 + \beta - \gamma D - \gamma P'_i) & \text{if } \phi \geq 0 \\ \beta - \gamma D - \gamma P'_i & \text{if } \phi < 0, \end{cases}$$

$$\frac{\mathrm{d}P_j}{\mathrm{d}t} = \frac{\mathrm{d}D}{\mathrm{d}t} + \frac{\mathrm{d}P'_j}{\mathrm{d}t} = \frac{\mathrm{d}P'_j}{\mathrm{d}t} = \begin{cases} (\alpha\phi^2 + \beta - \gamma D - \gamma P'_j) & \text{if } \phi \leq 0 \\ \beta - \gamma D - \gamma P'_j & \text{if } \phi > 0. \end{cases}$$

We now see that Equations (2) are equivalent to Equations (4), provided that $\beta - \gamma D = \beta'$. Furthermore, the initial conditions and threshold values must be adjusted according to the equations $P_i = D + P'_i$ and $P_j = D + P'_j$, yielding:

$$P'_{i,\text{init}} = P_{i,\text{init}} - D,$$

$$P'_{j,\text{init}} = P_{j,\text{init}} - D.$$

Therefore the PT model can be reformulated as a diffusive model, by choosing β' or D such that:

$$D = \frac{\beta - \beta'}{\gamma}; \quad P'_{i,\text{init}} = P_{i,\text{init}} - D; \quad P'_{j,\text{init}} = P_{j,\text{init}} - D;$$

$$P'_{i,\max} = P_{i,\max} - D; P'_{j,\max} = P_{j,\max} - D.$$

Equivalence between models can be used, for instance, to choose parameters for the diffusive models that allow canalization to start on its own, without the initial presence of carriers, and find the parameters of the equivalent FD and PT models.